Separation and Purification Technology 168 (2016) 19–31

Contents lists available at ScienceDirect

Separation and Purification Technology

journal homepage: www.elsevier.com/locate/seppur

Process optimization-based adsorbent selection for ethane recovery from residue gas

Libardo Estupiñan Perez, Adolfo M. Avila [1], James A. Sawada, Arvind Rajendran *, Steven M. Kuznicki

Department of Chemical and Materials Engineering, University of Alberta, 12th Floor, 9211-116 Street NW, Edmonton, Alberta T6G 1H9, Canada

ARTICLE INFO

Article history:
Received 8 November 2015
Received in revised form 3 May 2016
Accepted 9 May 2016
Available online 09 May 2016

Keywords:
Natural gas separation
Ethane extraction
Adsorption
Optimization
Titano-silicates
Pressure swing adsorption

ABSTRACT

The design and optimization of a pressure/vacuum swing adsorption process for the separation of ethane (C2) from residue gas (2.4 mol% ethane and the rest being methane) is presented. To achieve this, experimental measurements, modeling and optimization tools are developed to characterize the adsorbents, define the cycle configuration, and find the optimal operating conditions for the process. Adsorbents from two different families, namely, titano-silicate (Na-ETS-10) and activated carbons are chosen. Experimental high-pressure isotherms were measured and described using a dual-site Langmuir model. A rigorous one-dimensional model is developed to simulate the adsorption process. Two different pressure/vacuum swing adsorption (PVSA) cycle configurations are proposed and assessed based on C2 purity and recovery. The effect of feed temperature is studied and is shown to have a high impact on the separation. Finally, a multi-objective optimization study is performed to identify the material that offers the best trade-off between the two objective functions: C2 purity; and recovery. Among the adsorbents examined, Na-ETS-10 is found to provide the best performance with a possibility of obtaining ≈76% purity at a recovery of 68%.

1. Introduction

Natural gas (NG) is one of the most abundant and widely used fossil fuel. Recent technologies to extract shale and tight gas have increased the accessible reserves of natural gas [1,2]. In 2014, the U.S. Energy Information Agency (EIA) estimated the proven shale gas reserves of the world as nearly 2.7 trillion cubic metres (tcm), and the unproven resources to be greater than 200 tcm [3]. According to the EIA, shale gas will account for almost 50% of US domestic gas production by 2030. The increase of the NG reserves has caused a major impact on the chemical industry due to the cheaper prices of both natural gas and natural gas liquids (NGLs), i.e., ethane (C2) and heavier hydrocarbons. Due to its extensive use as a raw material to the manufacture of ethylene, C2 is one the most important components of NGLs.

Natural gas is a mixture of hydrocarbons and other impurities. While mainly methane (C1), the other hydrocarbons include C2, propane, and butane. Water, oil, sulfur, carbon dioxide, and nitrogen are typically found as impurities when extracted from the ground. These impurities are removed before the separation of NGLs from natural gas. Conventionally NGLs are separated from NG stream using a gas-subcooled process [4]. In this process, natural gas stream is compressed and rapidly expanded causing the gas temperature to drop significantly. This temperature drop allows for a cryogenic distillation of C1 from heavier hydrocarbons. This process allows for the recovery of ≈90 to 95% of the C2 originally in the gas stream. In addition, the expansion turbine uses some of the energy released when the natural gas stream is expanded in order to recompress the gaseous C1 effluent, thus saving energy associated with extracting C2. The extraction of NGLs from the natural gas stream produces cleaner natural gas, as well as the valuable hydrocarbons that are collectively referred to as NGL. The stream rich in C1 is usually called "residue gas" and its C1 composition is ~97–98 mol%. A small fraction of C2, which accounts for 2–3 mol%, is also present in the residue gas stream. The residue gas stream is primarily used as fuel. With the increasing demand for polyethylene and other chemicals, there is industrial interest in recovering and concentrating C2 from residue gas. The main objective of this paper is to study the separation of C2 from residue gas using pressure/vacuum swing adsorption (PVSA). The paper details material characterization, model-based process design and multi-objective optimization to study the

* Corresponding author.
E-mail address: arvind.rajendran@ualberta.ca (A. Rajendran).
[1] Current address: INQUINOA, Universidad Nacional de Tucumán, CONICET, DIPyGI-FACET-UNT, Av. Independencia 1800, C.P. 4000 San Miguel de Tucumán, Argentina.

http://dx.doi.org/10.1016/j.seppur.2016.05.010
1383-5866/

Nomenclature

A	cross-sectional area of the column [m^2]
b_0	parameter in Langmuir isotherm [$m^3\ mol^{-1}$]
c	fluid phase concentration
$C_{p,g}$	specific heat capacity of gas phase [$J\ mol^{-1}\ K^{-1}$]
$C_{p,a}$	specific heat capacity of adsorbed phase [$J\ mol^{-1}\ K^{-1}$]
$C_{p,s}$	specific heat capacity of adsorbent phase [$J\ kg^{-1}\ K^{-1}$]
$C_{p,w}$	specific heat capacity of column wall [$J\ kg^{-1}\ K^{-1}$]
D_m	molecular diffusivity [$m^2\ s^{-1}$]
d_0	parameter in Langmuir isotherm [$m^3\ mol^{-1}$]
L	column length [m]
h_{in}	inside heat transfer coefficient [$J\ m^{-2}\ K^{-1}\ s^{-1}$]
h_{out}	outside heat transfer coefficient [$J\ m^{-2}\ K^{-1}\ s^{-1}$]
k	mass transfer coefficient [s^{-1}]
K_z	effective gas thermal conductivity [$J\ m^{-1}\ K^{-1}\ s^{-1}$]
K_w	thermal conductivity of column wall [$J\ m^{-1}\ K^{-1}\ s^{-1}$]
n^{ads}	absolute amount adsorbed [$mol\ kg^{-1}$]
n^{ex}	excess adsorption [$mol\ kg^{-1}$]
P_H	high pressure [bar]
P_L	low pressure [bar]
P_{int}	intermediate pressure [bar]
q	solid phase concentration [$mol\ kg^{-1}$]
q^*	equilibrium solid phase concentration [$mol\ kg^{-1}$]
q_{sb}	saturation concentration in the solid phase for site 1 [$mol\ kg^{-1}$]
q_{sd}	saturation concentration in the solid phase for site 2 [$mol\ kg^{-1}$]
r_{in}	inner column radius [m]
r_{out}	outer column radius [m]
R	universal gas constant [$m^3\ Pa\ mol^{-1}\ K^{-1}$]
v_{feed}	interstitial feed velocity [$m\ s^{-1}$]
t	time [s]
T	temperature [K]
T_a	ambient temperature [K]
T_w	column wall temperature [K]
U	internal energy [$kJ\ mol^{-1}$]
V^a	volume of the adsorbed phase [m^3]
z	bed coordinate [m]

Greek symbols

ε	column void fraction [–]
ε_p	particle voidage [–]
ε_p	particle radius [m]
γ	adiabatic constant [–]
μ	fluid viscosity [$kg\ m^{-1}\ s^{-1}$]
ρ^a	density of the adsorbed phase [$kg\ m^{-3}$]
ρ^b	density of the bulk fluid phase [$kg\ m^{-3}$]
ρ_w	column wall density [$kg\ m^{-3}$]
τ'	tortuosity [–]
θ	reflux fraction [–]

Sub- and superscripts

ads	adsorption step
BD	blowdown step
Evac	evacuation step
feed	feed condition
HR	heavy reflux step
in	stream coming in
i	index of component
LPP	light product pressurization step
out	stream coming out

maximum achievable C2 purity and recovery. A key aspect considered in this work concerns the screening of different adsorbents for C2 recovery through rigorous process optimization.

2. Measurement and description of adsorption equilibria

2.1. Materials

Two different types of adsorbents were characterized in this study: a titanosilicate and carbons. Mixed coordination molecular sieves or titanosilicates (ETS) are micro-porous crystalline solids consisting mainly of an assemblage of titanium oxide (TiO_2) and silicate (SiO_2) [5,6]. The pore size in ETS-10 is uniform (~8 Å) and similar in dimension to large-pore classical zeolites. It is also known to have high thermal stability. ETS-10 has been used in previous studies to separate C2 from natural gas [7–10]. Na-ETS-10 was synthesized in-house and detailed preparation procedure has been reported in the literature [5,6]. Further, three commercial activated carbons were tested: Calgon BPL (referred to as BPL Carbon in this paper), Norit A powdered activated carbon by Cabot Corporation (referred to as Macro-Carbon), and 2GA activated carbon manufactured by Kuraray Chemical Corporation (referred to as Micro-Carbon). The adsorbent characteristics such as particle density and average pore size are summarized in Table 1. Particle density was obtained from the suppliers whereas average pore size was measured using an ASAP-2020 Physisorption Analyzer from Micromeritics. Unlike the carbon materials, which are commercial adsorbents with specified density values, Na-ETS-10 crystalline material was prepared in our lab. The pellets are normally prepared by mixing the synthesized material with a binder to be further compressed in a pellet press. The resulting disks have a density that can range approximately between ~900 and ~ 1100 kg/m^3 based on the characteristic of the synthesized material and the binder. The pressed disks are then grounded and sieved to 20–50 mesh. Therefore, a density value of 1000 kg/m^3 was selected as a representative particle density for Na-ETS-10 to be used in our simulations. In addition to the four materials characterized, two other carbons from the literature were used in the screening studies. They are labeled as AC1 [11] and AC2 [12], respectively. Methane and ethane with purities of 99.97% and 99%, respectively, purchased from Praxair were used to perform the experiments.

2.2. Experimental methods

Adsorption isotherms of C1 and C2 were measured using a high pressure volumetric adsorption analyzer (HPVA-100 from VTI scientific instruments) over a wide pressure range (up to 4000 kPa for C1 and up to 1000 kPa for C2). For the case of Na-ETS-10, six different temperatures, namely, 303.15 K, 323.15 K, 343.15 K, 373.15 K, 403.15 K, and 423.15 K were investigated. For the case of carbons, three temperatures were investigated, viz., 303.15 K, 323.15 K, 343.15 K.

The adsorption isotherms were measured based on the principle of volumetry. Briefly, the equipment consisted of a dose and a sample cell. The volumes of the cells were pre-calibrated. The adsorbent sample was placed in the sample cell and as a first experiment a known amount of Helium was dosed into the sample cell. By measuring the pressure on the sample side and by making an assumption that Helium is non-adsorbing, the "Helium volume", i.e., the difference between the empty volume of the cell and the skeletal volume of the adsorbent was measured. Although

Table 1
Properties of adsorbents characterized in this work.

Adsorbent	Particle density [kg/m^3]	Average pore size [Å]
Na-ETS-10	1000[a]	8
Micro-carbon	833	5
Macro-carbon	625	7
BPL carbon	766	13.9

[a] The pellet density ranges from ~900 to ~ 1100 kg/m^3. The average has been used for simulations.

Helium is known to adsorb on solids [13], it was ignored in this study as the operating pressures were relatively low compared to these pressures at which neglecting Helium adsorption has a major effect.

Once the Helium experiments are completed, the system was evacuated and the test gas was introduced in the cell. It is well known that, at any condition, the truly measurable equilibrium quantity is the excess adsorption [14]:

$$n^{ex} = V^a(\rho^a - \rho^b) \tag{1}$$

where V^a and ρ^a are the volume and density of the adsorbed phase, respectively, while ρ^b is the density of the bulk fluid phase. At low pressures $\rho^a \gg \rho^b$ and the excess amount reduces to

$$n^{ex} = n^{ads} = V^a\rho^a \tag{2}$$

where n^{ads} is the absolute amount adsorbed; a quantity that is traditionally used in the modeling of adsorption column dynamics. From Eq. (1), n^{ads} can be calculated from the measured n^{ex} using the expression

$$n^{abs} = n^{ex}\left(1 - \frac{\rho^b}{\rho^a}\right)^{-1} \tag{3}$$

Typically, for microporous adsorbents the density of the adsorbed phase is obtained from the slope of the descending portion of the excess isotherm plotted against the bulk fluid density. For systems where data at high pressure is not available, i.e., where a linear portion of the descending curve cannot be obtained, the liquid density at the boiling point is assumed to perform the conversion [15].

In the current work, the maximum bulk density of C1 corresponding to range of temperatures between 288.15 K and 423.15 K is 27.7 kg/m^3 to 27.4 kg/m^3. These values are much lower compared to the liquid phase density of C1 = 426 kg/m^3. Since ρ^b is reasonably small compared to ρ^a, the difference between n^{ex} and n^{ads} is a maximum of 7% at a temperature of 288.15 K and 4% for 423.15 K. Since this error is reasonably small, the measured n^{ex} values were considered to be absolute values. The measured isotherms are shown in Fig. 1.

2.3. Adsorption isotherms

The equilibrium isotherm data of C1 and C2 on the adsorbents considered in this study were fitted to a dual-site Langmuir model (DSL).

$$q_i^* = \frac{q_{sb,i}b_ic_i}{1 + \sum_{i=1}^{n_{comp}} b_ic_i} + \frac{q_{sd,i}d_ic_i}{1 + \sum_{i=1}^{n_{comp}} d_ic_i} \tag{4}$$

where $q_{sb,i}, q_{sd,i}, d_i$, and b_i are respectively the saturation capacities and affinity parameters for sites b and d, and c_i is the fluid phase concentration of component i. In the DSL model, the temperature dependence of b_i and d_i are described by the following expressions:

$$b_i = b_{0,i}e^{(-\Delta U_{b,i}/RT)} \tag{5}$$

$$d_i = d_{0,i}e^{(-\Delta U_{d,i}/RT)} \tag{6}$$

where $b_{0,i}$ and $d_{0,i}$ are the pre-exponential factors while $\Delta U_{b,i}$ and $\Delta U_{d,i}$ are the internal energy of adsorption. The DSL model has 6 parameters, $b_{0,i}, d_{0,i}, \Delta U_{b,i}, \Delta U_{d,i}, q_{sd,i}$, and $q_{sb,i}$, that should be fitted to the experimental data. In this work, parameters were obtained by simultaneous nonlinear regression of experimental isotherm data measured at different temperatures. The DSL parameters obtained for each adsorbent are shown in Table 2.

Using the DSL for binary systems raises an issue related with the appropriate combination of the affinity parameters (b_i and d_i) for the summation posed in the denominator of Eq. (4). This issue is important particularly in the case, such as the current situation, where experimental binary isotherms data is not available. Each component has two affinity parameters that should be combined with those of the second component in a particular way that it predicts the binary adsorption data well. Therefore, two possible combinations arise and an appropriate method to combine them is required. Ritter and coworkers showed, with experimental and predicted data, that for mixtures with similar properties, i.e., molecular size and adsorbent capacities such as C1–C2 a perfect positive (PP) correlation can describe with accuracy the binary adsorption [12]. A PP correlation implies that the sites are chosen in such a way than the higher values of the affinity coefficient are matched between the two components and the lower values are grouped together. This methodology was adopted in this work for all the adsorbents. The experimental equilibrium isotherm data along with the fitted isotherms are shown in Fig. 1.

3. Modeling and simulation of the adsorption process

In order to develop a mathematical model for a one-dimensional dynamic column, the following assumptions were made:

- The bulk fluid flow is represented using an axially dispersed plug flow model.
- The gas phase obeys the ideal gas law. In the range of pressures and temperatures studied in this work, the gas compressibility ranges from 0.99 to 0.96. Thus, assuming the fluid phase to be an ideal gas is reasonable.
- Mass transfer kinetics within the solid phase can be described by the linear driving force (LDF) model and the adsorption kinetics is controlled by the resistance to diffusion in the macropores.
- Darcy's law is used to describe the pressure drop in the axial direction.
- Bed voidage and particle size are uniform across the column.
- The fluid and adsorbent are in thermal equilibrium.
- Temperature, pressure, and concentration gradients in the radial direction are neglected.
- The outer column wall is in equilibrium with ambient temperature.

Under these assumptions, mass, energy, and transport equations can be derived and are shown in Table 3 [16,17].

The system of partial differential equations were converted to a non dimensional form and by using the finite volume method, the equations were discretized in space. The resulting coupled ordinary differential equations were solved using an in-built Matlab solver *ode23s*. In all the simulations, 30 volume elements, a balance between efficiency and computational speed, were used. At the beginning of the simulation, the column was considered to be saturated with 100% C1. A cycle implies the simulation of each step of the PVSA once in a specific sequence. The state of the column at the end of a step was taken as the initial condition for the subsequent step. The parameters for the model simulation

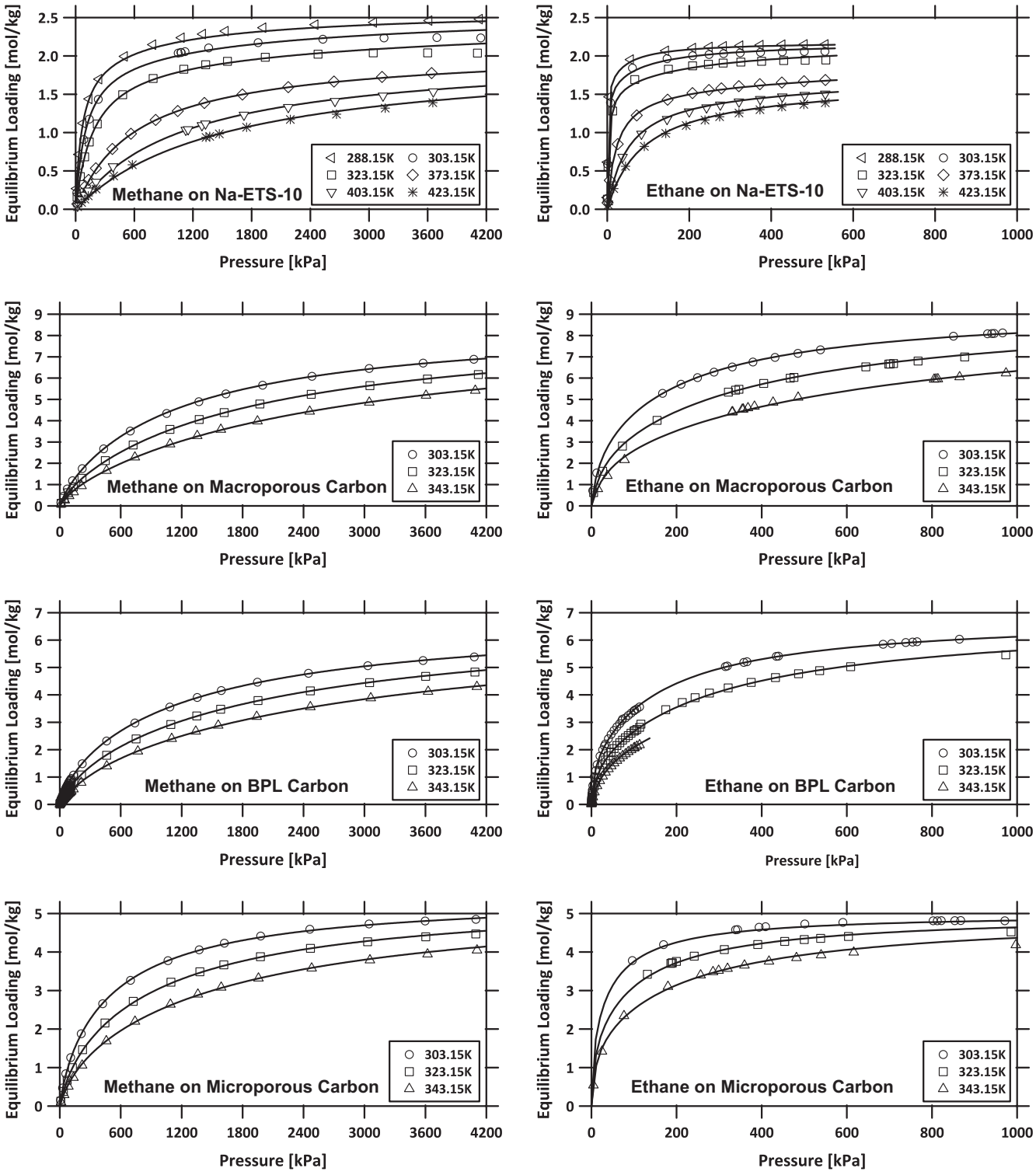

Fig. 1. Absolute adsorption isotherms of C1 and C2 on various adsorbents measured in this study. Symbols and lines represent experimental and fitted values, respectively.

can be found in Table 4. For cycles that involve reflux/recycle or feed from another column, the product from a certain column was collected in a well mixed tank and the mixed gas was used to pressurize/recycle to the receiving column. Since adsorption involves discrete switching, the simulation of many cycles was required in order to reach cyclic steady state (CSS) condition. The simulations were run for a minimum of 60 cycles after which the CSS mass balance criterion was checked. For the system described in this work, the number of cycles required to reach CSS varied between 60 and 100 cycles. At the end of the study a few configurations were considered and the process was simulated up to 500 cycles. The difference between the purity and recovery values calculated when the CSS criterion was satisfied and at 500 cycles was a maximum of 2.5 percentage points. The attainment of cyclic steady state was decided by computing the mass balance error defined as:

Table 2
Dual-site Langmuir parameters for adsorbents considered in this study.

Adsorbent	Comp.	$q_{sb,i}$ [mol/kg]	$q_{sd,i}$ [mol/kg]	$b_{0,i}$ [m^3/mol]	$d_{0,i}$ [m^3/mol]	$-\Delta U_{b,i}$ [kJ/mol]	$-\Delta U_{d,i}$ [kJ/mol]
Na-ETS-10	C1	0.630	1.981	1.010×10^{-9}	5.857×10^{-6}	35.061	21.132
	C2	0.602	1.584	2.234×10^{-8}	3.256×10^{-6}	35.508	33.252
Macro carbon	C1	0.670	8.059	5.077×10^{-3}	4.878×10^{-6}	4.124	15.283
	C2	2.386	6.974	3.414×10^{-4}	7.900×10^{-7}	15.551	24.273
Micro carbon	C1	1.015	4.459	5.271×10^{-4}	1.614×10^{-6}	10.074	19.790
	C2	1.578	3.420	4.036×10^{-4}	7.590×10^{-7}	19.025	27.813
BPL carbon	C1	1.188	5.715	6.358×10^{-5}	4.080×10^{-6}	14.096	15.378
	C2	1.462	5.429	1.125×10^{-6}	2.090×10^{-6}	32.923	22.454
AC1	C1	5.824		1.918×10^{-6}		16.633	
	C2	5.474		5.611×10^{-7}		25.102	
AC2	C1	5.300	3.910	2.413×10^{-6}	7.730×10^{-6}	11.331	15.484
	C2	3.330	4.460	3.331×10^{-7}	4.176×10^{-6}	19.133	23.382

Table 3
Equations for modeling adsorption column dynamics.

Overall mass balance	$\frac{1}{P}\frac{\partial P}{\partial t} - \frac{1}{T}\frac{\partial T}{\partial t} = -\frac{T}{P}\frac{\partial}{\partial z}\left(\frac{P}{T}v\right) - \frac{1-\epsilon}{\epsilon}\frac{RT}{P}\sum_{i=1}^{n_{comp}}\frac{\partial q_i}{\partial t}$
Component mass balance	$\frac{\partial y_i}{\partial t} + \frac{y_i}{P}\frac{\partial P}{\partial t} - \frac{y_i}{T}\frac{\partial T}{\partial t} = \frac{T}{P}D_L\frac{\partial}{\partial z}\left(\frac{P}{T}\frac{\partial y_i}{\partial z}\right) - \frac{T}{P}\frac{\partial}{\partial z}\left(\frac{y_i P}{T}v\right) - \frac{RT}{P}\frac{1-\epsilon}{\epsilon}\frac{\partial q_i}{\partial t}$
Mass transfer rate	$\frac{\partial q_i}{\partial t} = k_i(q_i^* - q_i)$
Pressure drop	$-\frac{\partial P}{\partial z} = \frac{150}{4}\frac{1}{r_p^2}\left(\frac{1-\epsilon}{\epsilon}\right)^2\mu v$
Column energy balance	$\left[\frac{1-\epsilon}{\epsilon}\left(\rho_s C_{ps} + C_{pa}\sum_{i=1}^{n_{comp}} q_i\right)\right]\frac{\partial T}{\partial t} = \frac{K_z}{\epsilon}\frac{\partial^2 T}{\partial z^2} - \frac{C_{pg}}{R}\frac{\partial}{\partial z}(vp) - \frac{C_{pg}}{R}\frac{\partial P}{\partial t} - \frac{1-\epsilon}{\epsilon}C_{pa}T\sum_{i=1}^{n_{comp}}\frac{\partial q_i}{\partial t} + \frac{1-\epsilon}{\epsilon}\sum_{i=1}^{n_{comp}}\left((-\Delta H_i)\frac{\partial q_i}{\partial t}\right) - \frac{2h_{in}}{\epsilon r_{in}}(T - T_w)$
Wall energy balance	$\rho_w C_{pw}\frac{\partial T_w}{\partial t} = K_w\frac{\partial^2 T_w}{\partial z^2} + \frac{2r_{in}h_{in}}{r_{out}^2 - r_{in}^2}(T - T_w) - \frac{2r_{out}h_{out}}{r_{out}^2 - r_{in}^2}(T_w - T_a)$

Table 4
Parameters used in the process simulation.

Simulation parameters		Value	
Column length	L	1	[m]
Column inner radius	r_{in}	0.1445	[m]
Column outer radius	r_{out}	0.1620	[m]
Column void fraction	ε	0.39	[–]
Particle voidage	ε_p	0.35	[–]
Particle radius	r_p	7.50×10^{-4}	[m]
Particle tortuosity	τ'	3	[–]
Column wall density	ρ_s	7800	[kg/m^3]
Specific heat capacity of gas phase	$C_{p,g}$	40.02	[J mol^{-1} K^{-1}]
Specific heat capacity of adsorbed phase	$C_{p,a}$	40.02	[J mol^{-1} K^{-1}]
Specific heat capacity of adsorbent	$C_{p,s}$	1070	[J kg^{-1} K^{-1}]
Specific heat capacity of column wall	$C_{p,w}$	502	[J kg^{-1} K^{-1}]
Fluid viscosity	μ	1.317×10^{-5}	[kg m^{-1} s^{-1}]
Molecular diffusivity	D_m	1.53×10^{-5}	[m^2 s^{-1}]
Adiabatic constant	γ	1.4	[–]
Effective gas thermal conductivity	K_z	0.0044	[J m^{-1} K^{-1} s^{-1}]
Thermal conductivity of column wall	K_w	16	[J m^{-1} K^{-1} s^{-1}]
Inside heat transfer coefficient	h_{in}	8.6	[J m^{-2} K^{-1} s^{-1}]
Outside heat transfer coefficient	h_{out}	2.5	[J m^{-2} K^{-1} s^{-1}]
Universal gas constant	R	8.314	[m^3 Pa mol^{-1} K^{-1}]
Operating conditions			
Interstitial feed velocity	v_{feed}	1	[m s^{-1}]
High pressure	P_H	2400	[kPa]
Low pressure	P_L	10	[kPa]
Intermediate pressure	P_{int}	50	[kPa]
Ambient temperature	T_a	298.15	[K]

$$\text{mass balance error} = \frac{|\text{mass}_{in} - \text{mass}_{out}|}{\text{mass}_{in}} * 100 \quad (7)$$

where mass_{in} and mass_{out} are the total amount of mass entering and leaving the process. If the mass balance error was below 1% for 5 consecutive cycles, it was assumed that the process has reached cyclic steady state and the simulation was stopped.

4. Cycle configuration

The separation problem studied here involves the concentration of a trace heavy-component (C2). The main objective is to maximize both purity and recovery of C2 in the product stream. In order to accomplish this two cycle configurations, found in literature to separate a heavy component, were implemented in this work

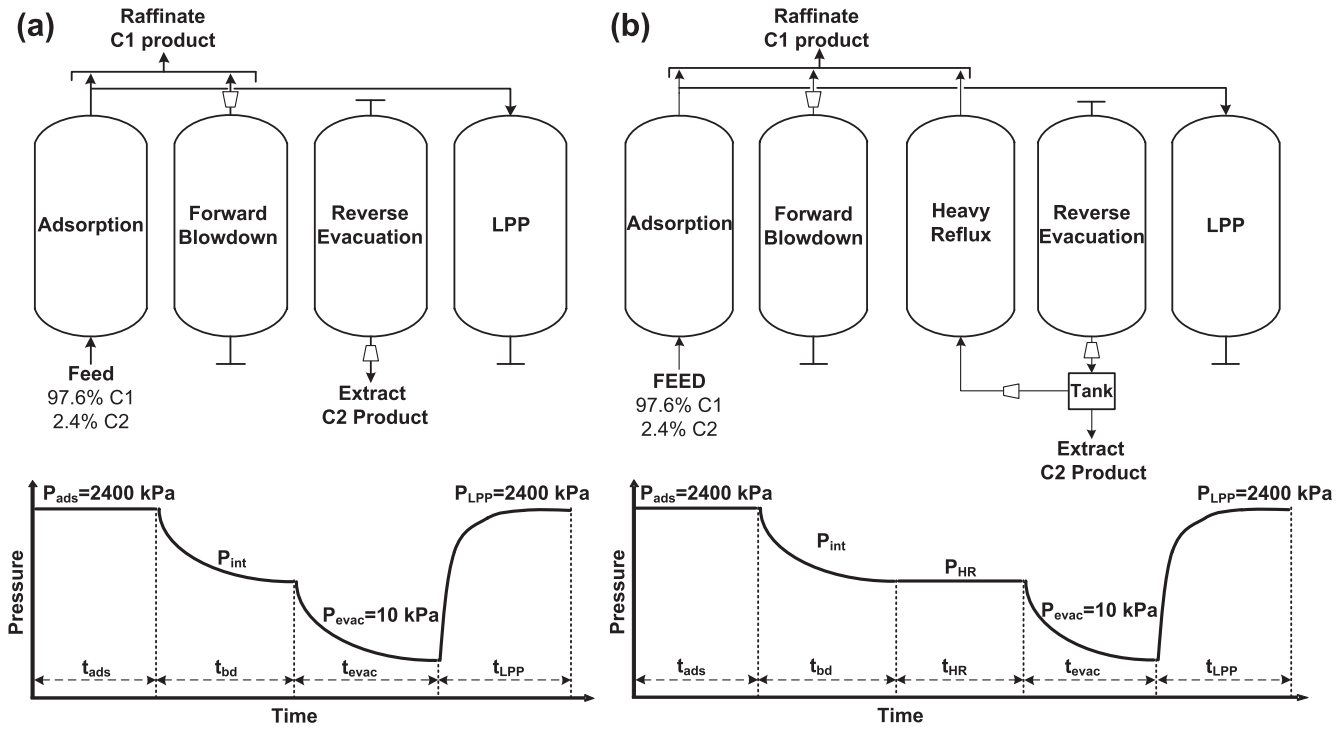

Fig. 2. Cycle configuration and process conditions. (a) Basic 4-step with light product pressurization (LPP); (b) 5-step with LPP and heavy reflux (LPP + HR).

[18]. A basic 4-step cycle with light product pressurization (LPP), and a 5-step cycle with light product pressurization and heavy reflux (LPP + HR), shown in Fig. 2, were chosen.

In this study C2 Purity (Pu) and Recovery (Re) were considered to be the primary indicators of process performance and are defined as follows:

$$\text{Purity (Pu)} = \frac{\text{moles of C2 in extract stream collected in 1 cycle}}{\text{total moles of C1} + \text{C2 in extract stream collected in 1 cycle}} * 100 \tag{8}$$

$$\text{Recovery (Re)} = \frac{\text{moles of C2 in extract stream collected in 1 cycle}}{\text{total moles of C2 fed in 1 cycle}} * 100 \tag{9}$$

4.1. 4-step cycle with light product pressurization (LPP)

The 4-step cycle with LPP (shown in Fig. 2(a)) includes a high-pressure adsorption step followed by a forward blowdown to an intermediate pressure, P_{int} in order to remove C1. An evacuation step where the pressure is reduced from P_{int} to P_{evac} is introduced to concentrate the C2 product. Finally, the gas from the outlet of the adsorption step is used to pressurize the column back to P_{ads}. In the classical Skarstrom cycle, the column is pressurized with the feed. However, for a system such as the one considered here, feed pressurization leads to a loss of C2 in the raffinate. In order to overcome this limitation the pressurization is performed using the light product. The use of C1 to pressurize in the reverse direction changes the dynamics of the column mainly in two ways:

- The light product, C1, pushes the C2 present in the raffinate product end towards the feed end, thereby avoiding the loss during the adsorption step resulting in improved recovery.
- Since C2 is mainly concentrated at the feed end of the column ($z = 0$), the intermediate pressure for the blowdown step can be lower when compared to the Skarstrom cycle. It will increase the amount of C1 removed from the bed during blowdown step, thereby increasing the purity of C2 during evacuation step.

As mentioned above, the LPP uses the product from the adsorption step to pressurize the column. Hence, this effluent should be stored in a tank and use it for pressurization. To implement this step in the simulation, it is necessary to calculate both, total and component mass balances of the adsorption product stream during the entire time span of the adsorption step. Although component mole fractions change through time, it was assumed that at the end of the step, the product is perfectly mixed within the tank and a final mole fraction is calculated using the mass balance shown in Eq. (10).

$$\text{moles out} = \frac{A\epsilon}{R}\int_0^{t_{ads}} \frac{P_0 y_{(t),out}\, v_{(t)}}{T_{(t)}}\, dt \tag{10}$$

The C2 mole fraction in the tank is calculated from:

$$y_{C2|_{tank}} = \frac{\text{moles out } C_2|_{ads}}{\text{total moles out}|_{ads}} \tag{11}$$

It is worth noting that this methodology is routinely applied in PSA modeling with minor loss in accuracy [18–20]. Using this stream as feed, the LPP step is carried out in the same way as a pressurization step. When simulating the LPP cycle by using tanks that are used to collect and deliver product it is important to ensure that moles of gas needed for pressurization does not exceed

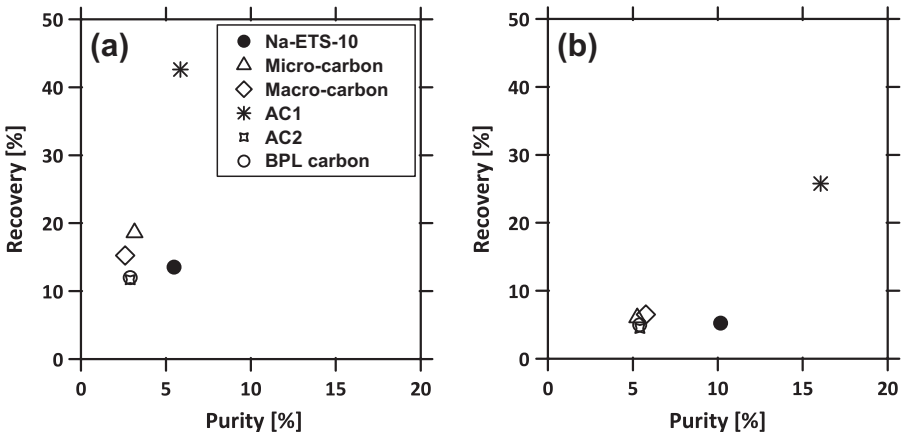

Fig. 3. Comparison of (a) LPP and (b) LPP + HR cycles at 298.15 K. Full list of operating conditions shown in Fig. 2.

that which was collected in the tank. If the tank is exhausted before completing the pressurization, the feed stream is used to complete the step and the recovery calculations are modified to consider this operation.

4.2. 5-step cycle with light product pressurization and heavy reflux (LPP + HR)

In this process configuration, shown in Fig. 2(b), a Heavy Reflux (HR) step is added to the configuration discussed above. The use of a HR step at the blowdown pressure (P_{int}) increases C2 purity while the LPP step increases its recovery. As shown in Fig. 2 (a), a fraction (θ) of the evacuation product is taken; stored in a tank; and refluxed into the column from the feed end ($z = 0$).

The HR step will cause the enrichment of the heavy component at the feed end of the column. C1 present in the gas and solid phases will be moved towards ($z = L$) and a product stream rich in this component will be obtained during the HR step. Furthermore, C2 purity in the evacuation step will increase because of both removal of C1 in HR step and C2 enrichment at the product end of the column. In terms of the simulation, HR step can be simulated as an adsorption step, but at low pressure. It implies that the same boundary conditions for the adsorption step are used also in the HR step, with the exception of the velocity. Once the number of moles collected in the tank is calculated, a reflux fraction is assumed and based on this value, the number of moles refluxed is calculated. The duration of the HR step (t_{HR}) and pressure, the inlet velocity is calculated as:

$$v_{HR} = \frac{\text{moles in C2}|_{\text{HR}}}{\text{t}_{HR} A \epsilon \frac{P|_{z=0}}{RT_{\text{feed}}|_{HR}}} \tag{12}$$

5. Results and discussion

5.1. Effect of light product pressurization and heavy reflux (LPP + HR) on process performance

Now that the column dynamics for each cycle has been explained, it is possible to proceed to discuss the simulation results. To compare the adsorbents, the conditions shown in Fig. 2 were used. Using these conditions, simulations of the two proposed cycles were performed for the six adsorbents described in Section 2 and shown in Fig. 3. It is clear from Fig. 3 that the best performance, at the conditions specified, is for AC1. Considering the isotherms of C1 and C2 on AC1 as shown in Fig. 1, it is noticeable that the isotherm for C2 on AC1 is less sharp when compared to the other adsorbents. Therefore, at a given evacuation pressure, AC1 is able to readily desorb C2 and thereby, resulting in increasing both purity and recovery. Further comparing Fig. 3(a) and (b), it is clear that the addition of a heavy-reflux step results in improvement of the purity, however, at the cost of the recovery. The effect on AC1 is particularly revealing as the purity increased from 7% to 16%.

5.2. Effect of temperature on process performance

The influence of temperature on the separation process was explored in an independent study and was determined to have a marked impact on the performance of the various adsorbents [21]. Higher temperatures reduce the non-linearity of the isotherms thereby facilitating desorption under vacuum. Three different feed temperatures, namely, 298.15 K, 343.15 K, and 373.15 K were used to study the impact of temperature. To verify this, simulations of the 5-step cycle with LPP + HR, the better of the two cycles, were performed for all the adsorbents at three different temperatures. The results of the simulations are depicted in Fig. 4.

From the figure, it can be seen that the increase of feed temperature enhances the performance of the cycle. All the adsorbents show better results at high temperatures. The improved performance can be attributed to the fact that C2 isotherm becomes less rectangular thereby aiding easy desorption of C2 during the evacuation step. It is possible to conclude from this results that adsorption capacity is not the sole indicator to choose adsorbents or to evaluate the performance. For example, the micro- and macro-carbons have higher adsorption capacity compared to Na-ETS-10. All adsorbents show similar performance at 298.15 K, but at higher temperature Na-ETS-10 exhibits a better performance.

In order to understand the reasons for the improved performance, it is important to analyze how the gas and solid phase profiles within the column change with the increase of feed temperature. With this purpose, gas and solid phase profiles of C2 using Na-ETS-10 as adsorbent are depicted in Fig. 5 for the operating conditions considered in Fig. 4. Since the blowdown and evacuation pressures are rather low, the purity of the C2 product depends mainly on the change in solid phase loading between these two steps. This is indicated as a shaded region in Fig. 4. At 298.15 K the solid phase profile shows that the adsorbent has a higher capacity when compared to the other two temperatures. However, the amount of C2 desorbed during the evacuation step, shown as a shaded region, is small due to the sharpness of the isotherm at this temperature which leads to a poor working capacity.

With the increase of feed temperature the adsorbent capacity decreases, as can be seen in the solid phase profiles at 343.15 K

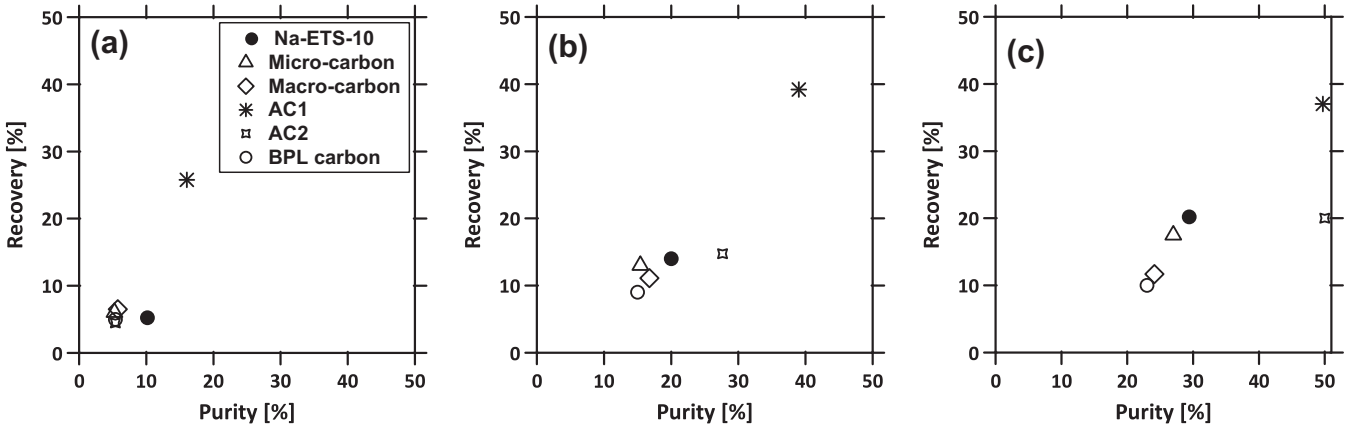

Fig. 4. The effect of feed temperature on the purity-recovery performance of six adsorbents undergoing a 5-step LPP + HR cycle. (a) 298.15 K; (b) 343.15 K; (c) 373.15 K.

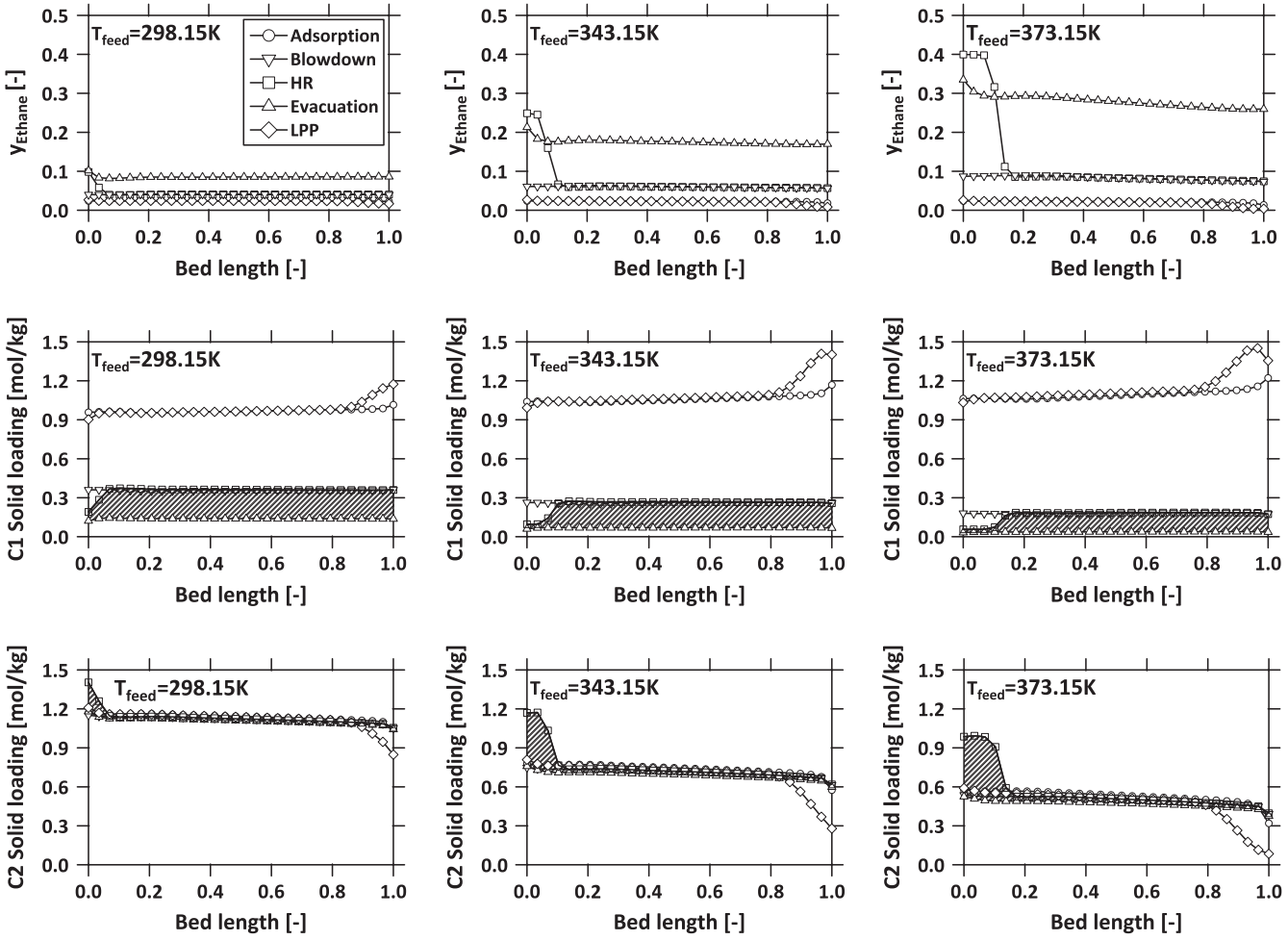

Fig. 5. Axial profiles of y_{C2}, solid loading of C1 and C2 at the end of the step corresponding to the 5-step cycle with LPP + HR at different feed temperatures using Na-ETS-10. The shaded region represents the amount of a particular species that is collected in the evacuation step. Operating conditions are shown in Fig. 2.

and 373.15 K from Fig. 5. Nevertheless, increasing temperature enhances the working capacity of the adsorbent since the sharpness of the isotherm is significantly reduced and hence, more C2 can be desorbed during the evacuation step. Fig. 5 shows how the increase in temperature enhance the material performance by increasing the amount of C2 desorbed during the evacuation step and reducing the amount of C1 present in the same step. A comparison of the column profiles shows that the amount of C2 desorbed at 343.15 K is ≈ three times compared to that of 298.15 K.

6. Material selection through optimization

Adsorbent screening is an important step in process development and various methods to screen adsorbents can be found in literature [22–25]. Methods found vary in complexity and many

Table 5
Optimization bounds for the 4-step LPP process and the 5-step LPP + HR process.

	t_{ads} [s]	t_{BD} [s]	t_{Evac} [s]	P_{int} [kPa]	P_{low} [kPa]	v_{feed} [m/s]	T_{feed} [K]
Lower bound	5	20	20	50	10	0.05	303.15
Upper bound	100	200	200	2400	40	2	423.15

metrics have been used to evaluate and compare their performance. Sorbent selection parameter (S) takes into account the thermodynamics of the system through selectivity and the adsorption–desorption pressures through the working capacity; thereby the product of these two metrics gives the parameter S [22,23]. The adsorbent with the highest S is expected to be the best adsorbent. Adsorbent Performance Indicator (*API*) takes into account three metrics, working capacity, selectivity and heat of adsorption along with three adjustable exponents which vary depending on the type of separation (bulk or trace component) [24]. Webley and coworkers developed a simplified 3-step PVSA cycle in order to evaluate the adsorbent performance for a specific gas mixture [25]. The method uses a simple adsorption–desorption–pressurization cycle taking into account heat effects for each step along with the specific work needed to pressurize and depressurize the column. In terms of reliability, this method can be considered to be intermediate to methods based only on metrics [22–24] and those that are based on rigorous adsorption simulation and optimization [16,18]. A recent study showed the correlation between performance metrics such as, selectivity and working capacity. on process performance [26]. In that work, the ability of these metrics to rank adsorbents was compared against a full process optimization approach. The study concluded that these metrics have a poor predictive capability of process performance since they do not take into account several aspects such as mass transfer resistances, heat effects, cycle configurations, and shape of the isotherm. Hence, the approach based on full process optimization is a more rigorous methodology to select adsorbents.

Most methods described in the literature seldom consider the complexity of the process to make comparisons. Further, very often processes are compared at sub-optimal conditions that do not provide an objective screening. Naturally, the main drawback of detailed process optimization is the excessive computational power that is required. However, recent developments in advanced numerical techniques, optimization algorithms, faster microprocessors, and the availability of reasonably priced computers with parallel processing capabilities allows performing these calculations within a few hours. Examples of this approach have been reported by our group and the efficacy of these method to predict experimental results at a pilot-plant scale have been demonstrated [16,18,27]. These methods provide the tools to objectively screen materials that take into account the process operation and increases the possibility of identifying the right candidate for further study.

6.1. Formulation of the optimization problem

As described in the introduction, the eventual industrial goal is to integrate the adsorption unit with the cryogenic distillation process. Optimizing the energy consumption of the entire unit, i.e., adsorption + cryogenic, is complex and beyond the scope of the current work. Hence, in this manuscript we limit our studies to the understanding of the trade-off between the purity and recovery of C2. In order to identify the optimal process conditions of the 4-step with LPP and the 5-step with LPP + HR, both optimization variables and process constraints should be defined before performing the multi-objective optimization. As for process constraints, adsorption and evacuation pressures are fixed based on the plant requirements and limitations. Adsorption pressure (P_H) and lowest vacuum pressure (P_L) are fixed at 2400 kPa and 10 kPa, respectively. The duration of the adsorption, blowdown and evacuation steps are considered decision variables as well as feed velocity (v_{feed}), feed temperature (T_{feed}), and intermediate or blowdown pressure (P_{int}).

To perform the optimization, a non-dominated sorting genetic algorithm II (NSGA-II) available in Matlab was used [28]. Advantages such as parallel computing, its implementation simplicity, its global search over a broad range of conditions, make the NSGA-II an appropriate algorithm for optimizing the PVSA process. All computations reported were carried out on a desktop workstation with two quad-core Intel Xeon 3.1 GHz processors and 128 GB RAM.

The population per generation was equal to 10 times the number of decision variables, a number considered adequately large enough to perform a full search of the process conditions. In this optimization problem the NSGA-II is run up to ≈100 generations. Although NSGA-II is not guaranteed to provide global minima, a distinct characteristic of genetic algorithm is its ability to consider points that are not essentially close to the optimum value. This adds diversity and hence, provides an opportunity to escape local minima.

6.2. Optimization of the 4-step cycle with LPP

For the optimization of the 4-step cycle with LPP, seven decision variables with their respective upper and lower bounds were established and are summarized in Table 5. As shown in Table 5, upper and lower bounds were defined in order to allow the optimizer to search in a broad range of process conditions. All the optimization variables chosen are considered critical for the process performance. For all the six adsorbents the same optimization bounds were used and the optimization routine was repeated for each of them. The Pareto fronts obtained for all of the materials obtained are shown in Fig. 6.

Before comparing the performance of the different adsorbents, it is worth considering the Pareto curve. The optimization problem considers simultaneously maximizing both purity and recovery of the heavy component (C2). Since purity and recovery are opposing performance indicators, they cannot be simultaneously improved. In other words, there is always a trade-off between the purity and recovery and the Pareto curve represents the best possible trade-off. The region towards the top right of any Pareto curve is infeasible while that towards the bottom left is sub-optimal. Hence, it is always desirable to operate the process on the Pareto curve. A key attraction of the optimization technique is that each point on the Pareto curve corresponds to a unique set of operating conditions, which will aid the operator to implement the process in practice.

Fig. 6 shows that Na-ETS-10 performs better than the other adsorbents in terms of C2 purity and recovery. The two carbons, AC1, AC2, micro- and macro-carbons follow Na-ETS-10. It is noteworthy than 100% recovery is achievable with all the sorbents making purity the decisive metric. To understand how the variation of the optimization variables affect the global performance of the process, it is necessary to analyze their variations with respect to one of the decision variables. To illustrate this, the

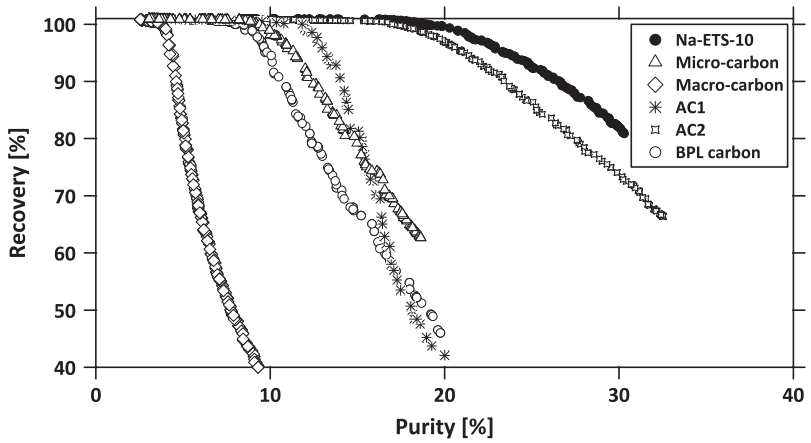

Fig. 6. Pareto fronts for various adsorbents tested for the 4-step cycle with LPP.

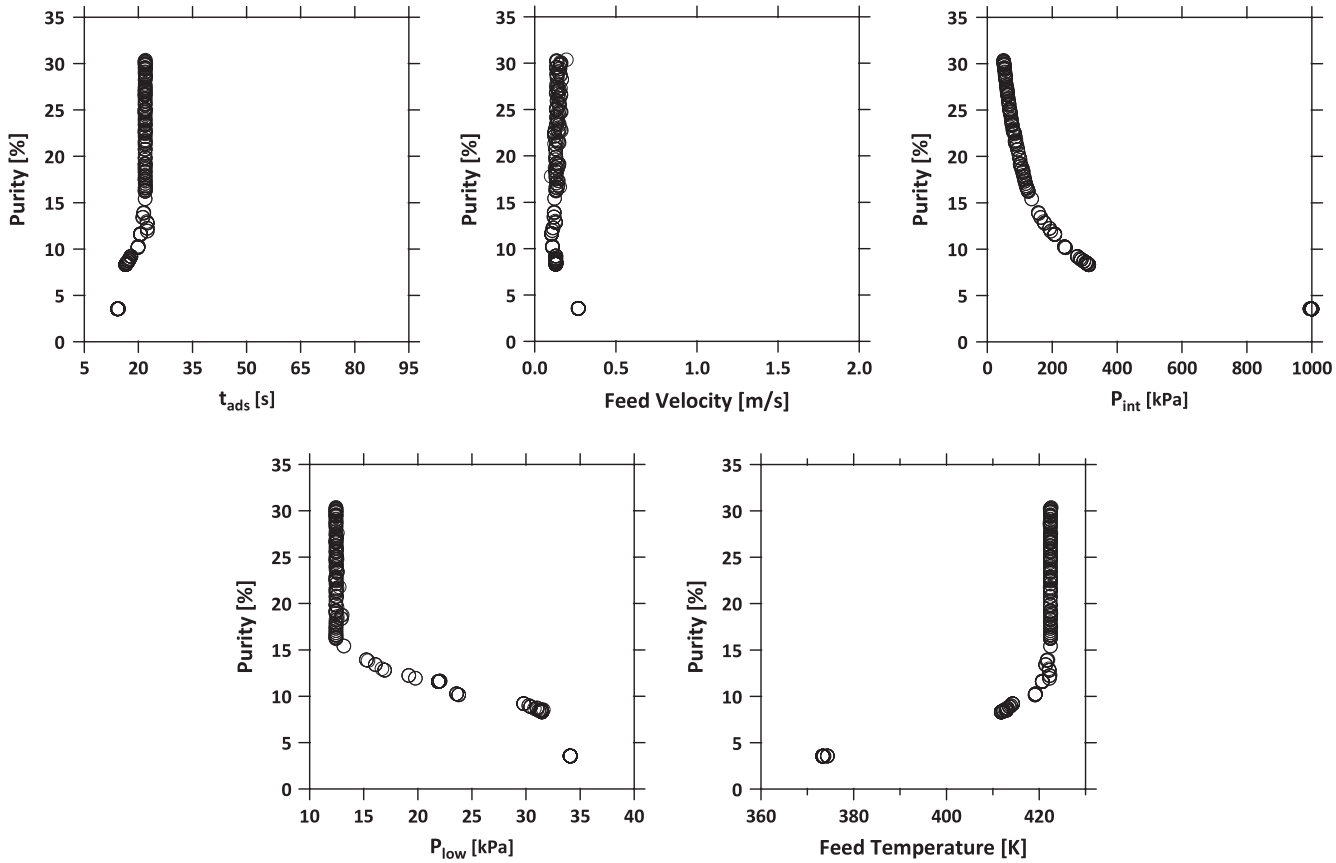

Fig. 7. Variation of decision variables with purity for the points on the Pareto curve for the optimization of a 4-step cycle with LPP employing Na-ETS-10. The range of the abscissa spans the lower and upper bounds of the decision depicted.

material with the best performance was chosen, i.e., Na-ETS-10. Fig. 7 depicts the behavior of the decision variables against purity for the points belonging to the Pareto front.

Analyzing each plot in Fig. 7, it can be seen that for the adsorption time (t_{ads}) the optimizer converged to one specific value ($\sim$ 20 s); this points out that above this value C2 will start breaking through leading to C2 loss. Feed velocity converges towards the lower bound for the entire range, suggesting a very slow movement of the C2 concentration front along the column, thereby avoiding losses of C2 during the adsorption step. As expected for both intermediate and low pressure (P_{int}, P_L), a decrease of their values will increase C2 purity substantially at the cost of recovery. The feed temperature shows an interesting trend. To maximize recovery a lower value of temperature is suggested whereas purity maximization is achieved at higher temperatures. It can be explained by the fact that at lower temperatures the isotherm is sharper and the amount of C2 loss during the blowdown step is less than at higher temperatures. As for purity, at higher temperatures, the isotherm is less non-linear and the amount of C2 withdrawn during the evacuation step is significantly higher than at lower temperatures.

6.3. Optimization of the 5-step cycle with LPP + HR

For the optimization of the 5-step cycle with LPP + HR, the low pressure P_{low} was fixed at its lowest value, i.e., 10 kPa. Further-

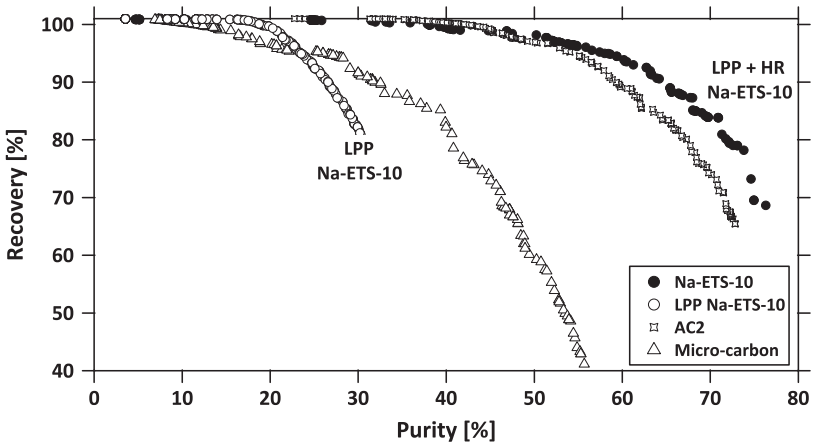

Fig. 8. Comparison of Pareto fronts for various adsorbents undergoing a 5-step cycle with LPP and HR.

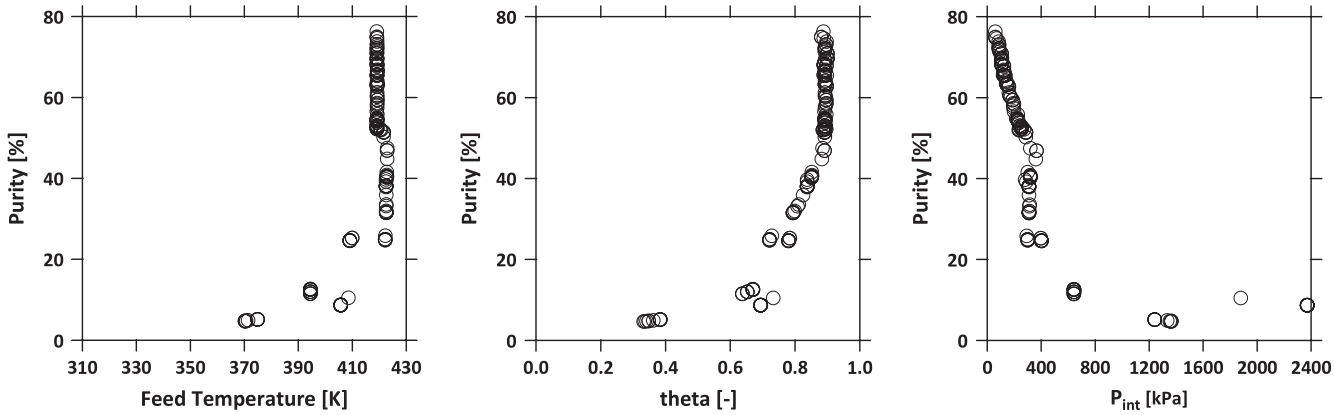

Fig. 9. Variation of selected decision variables as a function of C2 purity corresponding to the Pareto front of the 5-step PVSA cycle with LPP + HR. The plots correspond to Na-ETS-10.

more, two new decision variables, the reflux fraction (θ), and the time of the heavy reflux step (t_{HR}), were added. The lower and upper bounds for the reflux fraction were fixed at 0.1 and 0.9, respectively. As for the time of the heavy reflux step (t_{HR}), the bounds were set between 5 and 20 s. The rest of the decision variables taken into account for the optimization and their lower and upper bounds are described in Table 5.

For the optimization of this cycle, three adsorbents, Na-ETS-10, AC2 and micro-carbon, were selected based on the results obtained in the previous section. Optimization runs were carried out for the three adsorbents mentioned above and their respective Pareto fronts are depicted in Fig. 8. It is observed that the Pareto fronts for the 5-step cycle with LPP + HR have the same trend as those of the 4-step cycle with LPP, i.e., Na-ETS-10 has the best performance in terms of the objective functions, followed by the AC2 and the Micro-carbon. This result seems to confirm observations from literature that if one adsorbent performs better than the other for a specific system using a simple cycle configuration, the same adsorbent will perform better in more complex cycle configurations [25]. Nonetheless, more rigorous work is needed to ascertain this general observations.

In order to illustrate the effect of the HR step, the Pareto front for Na-ETS-10 from the LPP process is also shown in Fig. 8. The addition of a HR step shows a major impact on the process. For instance, at 80% recovery the C2 purity can be improved from ~30% to ~72% by the addition of HR step. This step is analogous to the reflux in a distillation column; thereby if the reflux fraction is increased, the purity of the heavy product during the evacuation step also increases [18]. Refluxing heavy product before the evacuation step increases its concentration at the feed end, i.e., $z = 0$. Additionally, the reflux pushes the light component from the feed end towards the product end of the adsorption column.

Using the Pareto front of Na-ETS-10, the decision variables were plotted against C2 purity in Fig. 9. The feed temperature shown in Fig. 9 yields a similar trend as in Fig. 7, i.e., higher temperatures favor higher purity, while lower temperatures favor recovery. High temperature reduces the sharpness of the isotherm; hence, more C2 can be released during the evacuation step. The reflux fraction (θ) follows the expected trend, i.e., as the reflux fraction increases purity also increases. Above a purity of 50%, the feed temperature and θ do not change considerably and the purity increase beyond this value is determined primarily by the intermediate pressure as shown in Fig. 9.

To compare the performance of the three adsorbents, a point for each adsorbent at identical recovery value from the Pareto fronts was taken. The operating conditions for these points are provided in Table 6. Note that for the case of Na-ETS-10 the optimizer converges to a low intermediate pressure of 59 kPa. This ensures that bulk of the C1 is removed in the blowdown step which is clearly seen in the concentration profiles shown in Fig. 10. It is worth noting that even at 59 kPa, Na-ETS-10 shows the capacity to retain C2 on the solid phase but is able to desorb it at the low pressure of 10 kPa. This results in a high C2 purity. In contrast, for the case of the micro-carbon, the optimizer converges on a P_{int} of 197 kPa. Lowering the pressure any further will lead to a loss of C2 recovery. Owing to this much of C1 and C2 remain on the solid phase and

Table 6
Process conditions at same recovery from the Pareto fronts for Na-ETS-10, AC2, and micro carbon.

Adsorbent	t_{ads} [s]	t_{BD} [s]	t_{Evac} [s]	t_{HR} [s]	P_{int} [kPa]	P_{low} [kPa]	v_{feed} [m/s]	T_{feed} [K]	θ [–]	Purity [%]	Recovery [%]
Na-ETS-10	19.76	39.29	60.93	6.57	59	10	0.15	419.09	0.88	76.29	68.6
AC2	34.17	40.26	131.47	10.15	167	10	0.12	405.33	0.89	71.80	68.5
Micro carbon	28.78	66.00	48.52	9.39	197	10	0.15	422.09	0.89	46.32	68.57

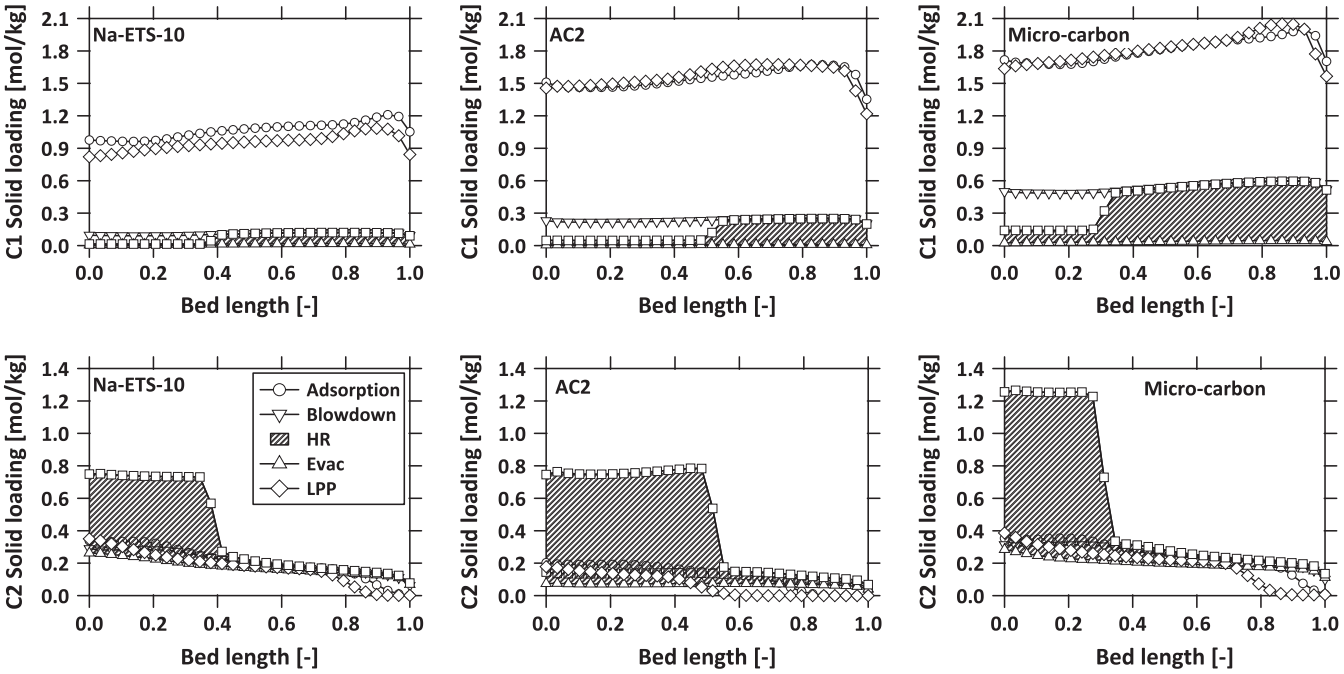

Fig. 10. Axial profiles of solid loading of C1 and C2 at the end of the step corresponding to the 5-step cycle with LPP + HR for three adsorbents. The shaded region represents the amount of a particular species that is collected in the evacuation step. The operating conditions are given in Table 6.

during the evacuation step, they are both desorbed resulting in lower purity. Hence, the superior performance of Na-ETS-10 seems to arise from its C2 isotherm non-linearity which ensures that C2 is still retained at a lower pressure, while C1 can be removed, resulting in better values of purity.

7. Conclusions

In this paper, modeling and optimization tools have been used to evaluate both the potential of different adsorbents and the PSA cycle configurations proposed for the separation of C2 from residue gas. Different adsorbents were tested and their experimental isotherm data was measured in-house and then, fitted to a dual-site Langmuir model. A full PSA model based on a finite volume discretization was implemented to simulate two cycle configurations designed for the recovery and concentration of the heavy component. Further, the full PSA model was coupled with a multi-objective optimizer based on the evolutionary methods in order to obtain a full purity-recovery Pareto front, which provides key answers about the best adsorbent, best cycle configuration, and optimized process conditions that maximize C2 purity and recovery. Two cycle configurations with light product pressurization (LPP) and heavy reflux with light product pressurization (LPP + HR) were implemented using the model developed. Simulations of the proposed PSA configurations using all the adsorbents showed that the addition of the LPP step increases the recovery of the heavy component whereas the addition of the HR enhances the C2 purity. Furthermore, it was determined for all the adsorbents considered in this study, that high feed temperatures are beneficial for the adsorbent performance due to the change in the isotherms shape, making them less sharply curved and hence, increasing the amount C2 desorbed during the evacuation step.

Using C2 purity and recovery as objective functions and operating conditions as decision variables, the multi-objective optimization was carried out using a non-dominated sorting genetic algorithm (NSGA-II). The multi-objective optimization provides a rigorous criterion for the screening of adsorbents and the best cycle configuration. For the cases studied, Na-ETS-10 showed the best performance in terms of purity and recovery.

Acknowledgements

Funding support from NSERC/NOVA Chemicals Industrial research chair program, NSERC Engage Grant EGP 452647-13 is acknowledged. The authors acknowledge the contributions of David Ting, Lee Henderson and Mohammad Keshtkar, NOVA Chemicals Corporation.

References

[1] U. EIA, Annual Energy Outlook With Projections 2014, U.S. Department of Energy, Washington D.C., 2014.
[2] Q. Wang, X. Chen, A.N. Jha, H. Rogers, Renew. Sustain. Energy. Rev. 30 (2014) 1–28.
[3] M. Melikoglu, Renew. Sustain. Energy. Rev. 37 (2014) 460–468.
[4] W.L. Luyben, Ind. Eng. Chem. Res. 52 (31) (2013) 10741–10753.
[5] M.W. Anderson, O. Terasaki, T. Ohsuna, A. Philippou, S.P. MacKay, A. Ferreira, J. Rocha, S. Lidin, Nature 367 (6461) (1994) 347–351.
[6] S.M. Kuznicki, Large-pored crystalline titanium molecular sieve zeolites, U.S. Patent 5011591A, 1991.

[7] N. Magnowski, A. Avila, C. Lin, M. Shi, S. Kuznicki, Chem. Eng. Sci. 66 (8) (2011) 1697–1701.
[8] S. Kuznicki, A. Avila, M. Shi, V. Strom, P. Herrera, Removal of ethane from natural gas at high pressure, U.S. Patent 20110315012 A1, 2011.
[9] N.A. Al-Baghli, K.F. Loughlin, J. Chem. Eng. Data 51 (1) (2006) 248–254.
[10] A. Avila, F. Yang, M. Shi, S. Kuznicki, Chem. Eng. Sci. 66 (13) (2011) 2991–2996.
[11] A. Malek, S. Farooq, AIChE J. 42 (11) (1996) 3191–3201.
[12] J.A. Ritter, S.J. Bhadra, A.D. Ebner, Langmuir 27 (8) (2011) 4700–4712.
[13] A. Rajendran, T. Hocker, O. Di Giovanni, M. Mazzotti, Langmuir 18 (25) (2002) 9726–9734.
[14] S. Sircar, AIChE J. 47 (5) (2001) 1169–1176.
[15] R. Pini, Micropor. Mesopor. Mater. 187 (2014) 40–52.
[16] R. Haghpanah, A. Majumder, R. Nilam, A. Rajendran, S. Farooq, I.A. Karimi, M. Amanullah, Ind. Eng. Chem. Res. 52 (11) (2013) 4249–4265.
[17] F.A. Da Silva, J.A. Silva, A.E. Rodrigues, Adsorption 5 (3) (1999) 229–244.
[18] R. Haghpanah, R. Nilam, A. Rajendran, S. Farooq, I.A. Karimi, AIChE J. 59 (12) (2013) 4735–4748.
[19] S.P. Reynolds, A.D. Ebner, J.A. Ritter, Ind. Eng. Chem. Res. 45 (12) (2006) 4278–4294.
[20] B.-K. Na, H. Lee, K.-K. Koo, H.K. Song, Ind. Eng. Chem. Res. 41 (22) (2002) 5498–5503.
[21] A. Avila, L. Estupinan-Perez, J. Sawada, A. Rajendran, Sep. Purif. Technol. (2015). in preparation.
[22] S.U. Rege, R.T. Yang, Sep. Sci. Technol. 36 (15) (2001) 3355–3365.
[23] R.T. Yang, Adsorbents: Fundamentals and Applications, Wiley Interscience, Hoboken, N.J., 2003.
[24] A.D. Wiersum, J.-S. Chang, C. Serre, P.L. Llewellyn, Langmuir 29 (10) (2013) 3301–3309.
[25] B.J. Maring, P.A. Webley, Int. J. Greenhouse Gas Control 15 (2013) 16–31.
[26] A.K. Rajagopalan, A.M. Avila, A. Rajendran, Int. J. Greenhouse Gas Control 46 (2016) 76–85.
[27] S. Krishnamurthy, V.R. Rao, S. Guntuka, P. Sharratt, R. Haghpanah, A. Rajendran, M. Amanullah, I.A. Karimi, S. Farooq, AIChE J. 60 (5) (2014) 1830–1842.
[28] K. Deb, A. Pratap, S. Agarwal, T. Meyarivan, IEEE Trans. Evol. Comput. 6 (2) (2002) 182–197.